Key role of chromophore-modified vibrational modes on thermal broadening of single-molecule spectra in disordered solids

Alexander O. Savostianov [1], Ivan Yu. Eremchev [1,2], Taras Plakhotnik [3], and Andrei V. Naumov [1,2,4]

[1] *Lebedev Physical Institute of the Russian Academy of Sciences, Troitsk Branch, Moscow, Troitsk 108840, Russia*

[2] *Institute of Spectroscopy of the Russian Academy of Sciences, Moscow, Troitsk 108840, Russia*

[3] *School of Mathematics and Physics, The University of Queensland, St. Lucia QLD 4072, Australia*

[4] *Moscow Pedagogical State University, Moscow 119435, Russia*

(Received 17 July 2023; revised 5 April 2024; accepted 21 June 2024; published 17 July 2024)

For decades, the thermal broadening of zero-phonon lines of single organic molecules embedded in amorphous solids was associated with their weak electron-phonon coupling to quasilocal vibrational modes. In this paper we show that the generally accepted perturbative approach for the pure dephasing problem is not applicable to the studied chromophore-doped glass, just as there is no evidence of weak coupling to individual quasilocal modes. Experimental and theoretical analysis of the temperature-dependent fluorescence excitation spectra of single tetra-*tert*-butylterrylene molecules in a polymer matrix of polyisobutylene is used as an example. Analysis of wide-range temperature measurements (9–60 K) with the nonperturbative theory of electron-phonon coupling demonstrates that the observed zero-phonon line broadening is due to the appearance of a wide spectrum of resonant modes induced by the impurity molecules themselves. This spectrum and the associated thermal broadening are obtained in the long-wave approximation for propagating waves using the density of the vibrational states for the host matrix and two quadratic coupling constants describing the interaction between the host and guest molecules. We also test the model considering the resonant modes arising from the host normal modes of a quasilocal character and find it completely incompatible with the experimental results.

DOI: 10.1103/PhysRevB.110.045430

I. INTRODUCTION

The phonon-induced optical dephasing resulting in homogeneous broadening of zero-phonon lines (ZPLs) has a great effect on optical properties of numerous emitters promising for nanophononics [1–5]. Among such emitters are also single organic molecules (SMs) embedded in solid matrices [6]. There is a growing interest in using SMs as single-photon emitters [7–9], or even as a platform for designing of integrated photonic circuits where SMs are coupled to waveguides or microresonators [10]. Although the well-ordered matrices, such as the molecular crystals, are the most widespread in these applications, polymers are also of interest due to the significant increase in microresonator performance when this type of matrix is used to cover the fabricated chips [11]. At the same time, for these tasks it is desirable to generate the lifetime-limited ZPLs, which is difficult to achieve for SMs in disordered matrices even at a temperature of a few degrees kelvin. It is well known that even at liquid helium temperatures the SM ZPLs are subject to optical dephasing induced by the interactions between the electronic states of the emitter and phononlike excitations, existing in solids [12]. Moreover, spectral diffusion (SD) resulting in random changes in the ZPL positions due to the interaction with two-level tunneling systems (TLSs) is also a problem [13,14].

Although optical dephasing has been a topic of detailed research for many decades, and the mechanism of quadratic coupling leading to the ZPL broadening is well understood [15–22], the question of which vibrational modes contribute to dephasing in the case of a particular emitter still arises regularly; as an example one can mention nitrogen-vacancy (NV) centers in diamonds [2,23]. The origin of dephasing in dye-doped polymers and glasses is also of interest. Various spectroscopic techniques, such as spectral hole burning, photon echo, and single-molecule spectroscopy, suggest that for organic molecules embedded in amorphous solids, only individual quasilocal modes (QLMs) with energies on the order of tens or even units of cm^{-1} contribute to dephasing, while other phonon modes are inactive, even above liquid nitrogen temperatures [24–29]. The physical reasons for such selective coupling over such a wide temperature range are not entirely clear. Furthermore, assuming that QLMs are intrinsic modes of the host material, the question arises as to whether it is possible to discover or to design an amorphous material in which these selective modes are suppressed.

It should be emphasized that the conclusions regarding the origin of dephasing in dye-doped glasses are typically based on the phenomenological second-order perturbation theory treating the ZPL broadening as an inelastic Raman-type process [30]. This approach was pioneered by McCumber and Sturge for the Debye model of acoustic phonons [15] and later extended to include QLMs [17]. Its main limitation is that it assumes *a priori* that the quadratic electron-phonon coupling leading to dephasing is weak, which is not at all obvious. Nevertheless, it is widely used because of its good agreement with experimental data for a variety of dye-doped glasses [12]; therefore, no special effort was made to justify the weak electron-phonon coupling. At the same time, a more

general nonperturbative Osad'ko–Skinner–Hsu (OSH) theory (developed by Osad'ko [18,31] and confirmed by Skinner and Hsu [19,32,33]) allows to consider electron-phonon coupling of arbitrary strength. Another advantage of the OSH theory is that the expressions for the ZPL broadening include the density of phonon states (DOS), which makes it relatively easy to test different models of phonon dynamics.

These considerations motivated us to apply single-molecule spectroscopy [6,34,35] to reexamine the temperature-dependent ZPLs of tetra-*tert*-butylterrylene (TBT) SMs embedded in a glassy matrix (polyisobutylene, or PIB for short). The goal of our study is to verify the accuracy of the established conclusions regarding the origin of phonon-induced dephasing in a dye-doped polymer. Since the perturbative expressions have limited applicability, we aim to verify the weak electron-phonon coupling between the dye molecule and the QLMs using the OSH nonperturbative theory of electron-phonon coupling. For this purpose, we measured fluorescence excitation spectra in a wide spectral range of $\sim$56 cm^{-1}, which was about 30 times larger than in the similar measurements in Refs. [27,36]. This allowed us to extend the range of investigated temperatures to 60 K, covering almost the entire temperature range where ZPLs of individual molecules in polymer hosts can be distinguished [37]. We obtained an interesting result: although some experimental data are reasonably described by the perturbative formula, the OSH theory refutes the existence of weak coupling with single QLMs in these cases. This finding motivated us to consider the distortion of the vibrational dynamics of glasses by the impurity and the optical dephasing caused by such distortion. We have studied the model of the so-called resonant modes (RMs) induced by the impurity molecules themselves and argue that this model is applicable to glasses. We demonstrate that the RM model is able to capture the observed dephasing within the long-wavelength approximation, which is commonly associated with propagating plane waves and in which the coupling strength scales proportionally to the square root of the mode frequency (that is, $\propto \omega^{1/2}$). However, the model fails if the scaling is assumed to be proportional to $1/\omega^{1/2}$, which corresponds to the quasilocalized nature of the host normal modes.

The paper is organized as follows. In Sec. II we discuss the theoretical treatment of electron-phonon coupling. In Secs. II A and II B we give an overview, introducing the dephasing effect on optical spectra, and then the OSH theory. In Sec. II C, we consider the SM-QLM coupling in the framework of the OSH approach, then derive the common perturbative formula and identify its limitations. An introduction to the concept of RMs and the adaptation of this model to dephasing in dye-doped glasses is given in Sec. II D. The experimental details are discussed in Sec. III. Section IV outlines the experimental findings of ZPL thermal broadening and their relation to various models of the electron-phonon coupling. Section IV A clarifies the interpretation of the measured spectra, while Sec. IV B provides a brief report on spectral diffusion. The main results are presented in Secs. IV C and IV D, where the observed dephasing is analyzed in the context of coupling with QLMs and RMs, respectively. In Sec. IV E, the prospects of the RM model are discussed, as well as its connection to other widely accepted models of dephasing.

II. THEORETICAL TREATMENT OF PHONON-INDUCED DEPHASING

A. Relation between optical dephasing and ZPL broadening

Although organic molecules have a complex system of electronic and vibrational levels, in terms of optical dephasing they can be treated as a two-level system in which only radiative transitions occur. The term *optical dephasing* in this paper refers specifically to pure dephasing, which does not involve population transfer [31]. In the case of electron-phonon interaction in impurity-doped solids, the motion of the host atoms randomly modulates the energy difference between the ground (S_0) and the electronically excited (S_1) states which results in the broadening of the optical $S_0 \rightarrow S_1$ transition. In this framework, the ZPL full width at half maximum (FWHM) $\gamma(T)$ is a sum of the inverse excited-state lifetime T_1 and the inverse pure dephasing time $T_2^{'}$ [31], that is

$$\gamma(T) = \frac{1}{\pi T_2} = \frac{1}{2\pi T_1} + \frac{1}{\pi T_2^{'}}, \tag{1}$$

where T_2 is the total dephasing time. It should also be noted that the ZPLs detected by the SM technique are subject to SD, which occurs on a timescale much longer than the dephasing time [38] and results from the interaction of SMs with a large number of TLSs [39,40] uniformly distributed throughout the glass volume. The following law of broadening arising from SD has been established phenomenologically [28]:

$$\gamma_{\mathrm{SD}}(T) = bT^a, \tag{2}$$

where b is a constant weakly affected by the measuring time and the depending on the host–guest systems; exponent a is between 1 and 2. Summing up, the total ZPL FWHM measured in SM experiments can be written as

$$\gamma_{\mathrm{ZPL}}(T) = \frac{1}{2\pi T_1} + bT^a + \gamma_{\mathrm{ph}}(T), \tag{3}$$

where $\gamma_{\mathrm{ph}}(T) = 1/(\pi T_2^{'})$ is the phonon-induced pure dephasing, which is the subject of this study. Typical values of $1/(2\pi T_1)$ are in the range of tens of megahertz (MHz) [10]; the SD contribution to ZPL broadening grows slowly both with temperature and measuring time and is typically limited by a few gigahertz (GHz) [28]. In turn, phonons induce a barely detectable dephasing below 4–5 K; however, at temperatures of about 15 K it is several times greater than the TLS contribution [41].

B. OSH theory of electron-phonon coupling

The OSH theory of the electron-phonon coupling [18,19,31] employs adiabatic and harmonic approximations when the vibrational Hamiltonian for the ground-state impurity is the sum of Hamiltonians of independent harmonic oscillators:

$$\hat{\mathrm{H}}_0 = \sum_k \hbar\omega_k \left(b_k^+ b_k^- + \frac{1}{2} \right), \tag{4}$$

where b_k^+ and b_k^- are, respectively, creation and annihilation operators of the kth phonon with energy $\hbar\omega_k$. The OSH theory considers a change in the vibrational Hamiltonian due to the chromophore electronic excitation. One can expand this change in a Taylor series using the ground-state normal-mode coordinates:

$$\hat{\mathrm{H}}_1 - \hat{\mathrm{H}}_0 = \mathrm{E}_0 + \hat{V} + \hat{W}, \tag{5}$$

where E_0 is a constant, $\hat{V} = \sum_k g_k(b_k^+ + b_k^-)$, and $\hat{W} = \sum_{k,q} g_{kq}(b_k^+ + b_k^-)(b_q^+ + b_q^-)$ are, respectively, linear and quadratic electron-phonon coupling operators depending on g_k and g_{kq}, which are the linear and quadratic coefficients in the Taylor series. Equation (5) can be significantly simplified by considering a single collective coordinate φ, which is a linear combination of normal-mode coordinates representing either local strain or a local coordinate [19]:

$$\hat{\Lambda} \equiv \hat{V} + \hat{W} = a\varphi + \tfrac{1}{2}W\varphi^2, \tag{6}$$

where

$$\varphi = \sum_k h_k(b_k^+ + b_k^-). \tag{7}$$

In this approximation, h_k are the expansion coefficients of the collective coordinate in normal modes, while a and W are the constants of linear and quadratic electron-phonon coupling, respectively. The consideration becomes significantly more complicated when several local coordinates are involved. This more complex case where $\hat{\Lambda} = \sum_i a_i\varphi_i + (1/2)\sum_{i,j} W_{i,j}\varphi_i\varphi_j$ and $\varphi_i = \sum_k h_{ik}(b_k^+ + b_k^-)$ [42] is not considered in this paper.

Within the Condon approximation, the absorption line shape of ZPL $I_{\mathrm{abs}}(\omega)$ reads

$$I_{\mathrm{abs}}(\omega) \sim \int_{-\infty}^{\infty} \exp[i(\omega-\omega_0)t]\exp\left(-\frac{|t|}{2T_1}\right)\langle F(t)\rangle dt, \tag{8}$$

where $F(t) = \exp(i\hat{H}_0 t/\hbar)\exp[-i(\hat{H}_0+\hat{\Lambda})t/\hbar]$. First Osad'ko and later Skinner and Hsu found that ZPL has a Lorentzian shape with FWHM as described by Eq. (1), where the phonon-induced dephasing $\gamma_{\mathrm{ph}}(T)$ is defined by the following expression [18,19,31]:

$$\gamma_{\mathrm{ph}}(T) = \frac{1}{2\pi}\int_0^{\infty} \ln\{1+4n(\omega) \times [n(\omega)+1]W^2\Gamma_0(\omega)\Gamma_1(\omega)\}d\omega. \tag{9}$$

Here, $n(\omega) = [\exp(\hbar\omega/kT)-1]^{-1}$ is the probability of finding phonons with frequency of ω and

$$\Gamma_{0,1}(\omega) = \pi\sum_k (h_k)^2\delta\left(\omega-\omega_k^{0,1}\right) \tag{10}$$

are the spectral phonon functions for the impurity S_0 and S_1 electronic states, respectively. In this paper we use wave numbers (cm^{-1}) as the units of ω and follow Osad'ko's normalization for $\Gamma_{0,1}(\omega)$:

$$\int_0^{\infty}\omega\Gamma_{0,1}(\omega)d\omega = \pi. \tag{11}$$

The relation between $\Gamma_0(\omega)$ and $\Gamma_1(\omega)$ is given by

$$\Gamma_1(\omega) = \frac{\Gamma_0(\omega)}{[1-W\Omega_0(\omega)]^2 + [W\Gamma_0(\omega)]^2}, \tag{12}$$

where

$$\Omega_0(\omega) = \frac{2}{\pi}\int_0^{\infty}\frac{\nu\Gamma_0(\nu)}{\omega^2-\nu^2}d\nu \tag{13}$$

is calculated in the Cauchy principal value.

Two important conclusions should be emphasized. First, in the absence of quadratic electron-phonon coupling ($W=0$), the phonon-induced dephasing disappears. Second, a single value of W implies a local character of the electron-phonon coupling. Taking into account the strong dependence of the intermolecular forces on distance, one can assume that the interaction with the nearest neighbors determines the value of W. One should also note that the OSH theory is applicable if the characteristic relaxation time of the phonon bath is much shorter than the pure dephasing time. The requirement for the timescale separation can be estimated in terms of coupling with the reservoir of acoustic phonons as follows [32]:

$$\gamma_{\mathrm{ph}}(T) \ll \frac{\omega_{\mathrm{D}}T}{T_{\mathrm{D}}}, \tag{14}$$

where ω_{D} is the Debye frequency, while T_{D} is the Debye temperature.

C. Coupling with quasilocalized modes

Coupling to a QLM is a purely phenomenological theory postulating the existence of a single vibrational mode with a finite lifetime and a Lorentzian shape of the spectral phonon function. We use the following $\Gamma_0(\omega)$ [43]:

$$\Gamma_0(\omega) = \frac{\gamma_0}{2\omega_0}\left[\frac{1}{(\omega-\omega_0)^2+(\gamma_0/2)^2} - \frac{1}{(\omega+\omega_0)^2+(\gamma_0/2)^2}\right], \tag{15}$$

where ω_0 is the QLM frequency when the molecule is in the S_0 state and γ_0 is the QLM inverse lifetime. Addition of a second Lorentzian centered at $\omega=-\omega_0$ does not change noticeably the Lorentzian shape, except when $\gamma_0 \gtrsim \omega_0$, but eliminates the divergence at $\omega\to 0$ in the integrand in Eq. (9), enables normalization of $\Gamma_0(\omega)$, and analytical calculation of $\Omega_0(\omega)$. It follows from Eqs. (12) and (13) that $\Gamma_1(\omega)$ has the shape of $\Gamma_0(\omega)$ with the substitution $\omega_1 = \sqrt{2W+\omega_0^2}$ for ω_0.

A simpler expression has been obtained using a perturbation theory (the so-called "weak-coupling limit"), which is usually applied to analyze QLM-induced dephasing [17]:

$$\gamma_{\mathrm{ph}}(T) = B\frac{\exp(-\hbar\bar{\omega}/kT)}{[1-\exp(-\hbar\bar{\omega}/kT)]^2}, \tag{16}$$

where $\bar{\omega}$ is the QLM frequency negligibly dependent on the chromophore electronic state, and B is a coupling constant. Mathematically, Eq. (16) is a limit of the OSH theory in the case of $W\to 0$, but this also leads to $\mathrm{B}\to 0$ and hence the broadening vanishes. Osad'ko presented a less strict criterion for the transition to the weak-coupling limit: $W/(\omega_0\gamma_0) \ll 1$ [18]. We find that this condition is necessary but not sufficient. Several additional assumptions, some of which are incompatible, are required to derive Eq. (16) from the OSH theory.

To define them, we consider $\Gamma_{0,1}(\omega)$ as functions with sharp peaks at slightly different frequencies $\omega_0 \approx \omega_1 \approx \bar{\omega}$

and with an effective width of $\Delta\omega$, defined by the equality $\int_0^\infty \omega\Gamma_{0,1}(\omega)d\omega = \bar{\omega}\Gamma_{0,1}(\bar{\omega})\,\Delta\omega$. The condition $\omega_0 \approx \omega_1 \approx \bar{\omega}$ implies that

$$|\omega_1 - \omega_0| \ll \Delta\omega. \tag{17a}$$

The linearization of the logarithm in Eq. (9) is valid if $4n(\omega)[n(\omega)+1]W^2\Gamma_0(\omega)\Gamma_1(\omega) \ll 1$. Defining $\gamma_{\rm ph}(T)$ according to Eq. (16), one can obtain this condition using experimentally measured value of the ZPL broadening:

$$\frac{4\pi\gamma_{\rm ph}(T)}{\Delta\omega} \ll 1. \tag{17b}$$

Finally, to take $n(\omega)[n(\omega)+1]$ out from the integral, the condition on the $\Gamma_{0,1}(\omega)$ sharpness is necessary. After some lengthy but simple algebra (see Appendix A), it is reduced to

$$\frac{\Delta\omega^2}{2\bar{\omega}^2}\left[4+\left(\frac{\hbar\bar{\omega}}{kT}\right)^2\right] \ll 1. \tag{17c}$$

If Eqs. (17a)–(17c) hold, the approximate expression for $\gamma_{\rm ph}$ reads exactly as Eq. (16) with $B = \pi W^2/(\bar{\omega}^2\Delta\omega)$ and $\bar{\omega} \approx (\omega_0+\omega_1)/2$.

If $\Gamma_0(\omega)$ is described by Eq. (15), then $\Delta\omega = \pi\gamma_0/2$. Taking into account the relation between ω_0, ω_1, and W, as well as the expression for B introduced above, we can rewrite criteria (17a)–(17c) as follows:

$$\frac{B}{\pi\gamma_0} \ll 1, \tag{18a}$$

$$\frac{8\gamma_{\rm ph}(T)}{\gamma_0} \ll 1, \tag{18b}$$

$$\left(\frac{\gamma_0}{\bar{\omega}}\right)^2\left[4+\left(\frac{\hbar\bar{\omega}}{kT}\right)^2\right] \ll 1, \tag{18c}$$

where

$$B = \frac{2W^2}{\bar{\omega}^2\gamma_0}. \tag{19}$$

Upon closer examination, it is evident that fulfillment of the criteria (18a)–(18c) is a challenging task. Inequality (18a) is obviously more accurate for larger γ_0, but the value of γ_0 is not included explicitly in Eq. (16). The values of γ_0 of the order of a few $\rm cm^{-1}$ were previously determined from the phonon sidebands (PSBs) for organic molecules in various hosts [29,44,45]. We roughly estimate the upper limit of $\Delta\omega$ as $\sim 4\pi$ $\rm cm^{-1}$ that corresponds to γ_0 of ~ 8 $\rm cm^{-1}$ and a QLM lifetime of ~ 0.7 ps. This estimate implies that the measured broadening according to Eq. (18b) must satisfy the inequality $\gamma_{\rm ph}(T) \ll 1$ $\rm cm^{-1}$, which makes the weak-coupling limit inapplicable for analyzing high-temperature data. At the same time, neither the large values of γ_0 nor the low temperatures favor condition (18c).

D. Coupling with resonant modes

The concept of QLM-induced dephasing seems to contradict the temperature broadening of the ZPL of impurity molecules in crystalline matrices (see, e.g., Ref. [20]), where the reservoir of acoustic phonons is coupled to the emitter. Although a weak coupling with QLMs is in agreement with the results of numerous experiments, the nature of such modes is unclear. There are two alternative descriptions of these modes (see Ref. [12] and references. therein). First, QLMs are the normal modes of glasses, which constitute the boson peak. Second, QLMs can also be considered as resulting from perturbations of the matrix normal modes caused by the impurity molecules. This hypothesis is supported by the fact that Eq. (16) can be accurate in some cases even for molecules embedded in well-ordered crystalline matrices [28], where the boson peak is not observed.

In line with the second hypothesis, we assume that impurity molecules can affect the normal modes of glasses in a similar way to how point defects locally modify the normal modes of ideal crystals. It is well known that such modification results in the appearance of vibrational resonance modes (RMs) [46]. These modes are expected either when an impurity is heavier than the host atoms or molecules [47], or when the bond between the impurity and the host is weaker than the bond between the host molecules themselves [48]. The conditions for the emergence of RMs seem to be satisfied when a guest molecule is incorporated into a glassy matrix of a significantly different structure. Therefore, RMs can be considered as the cause for ZPL broadening. Previously, the effect of RMs on various impurity centers in crystals was studied by Skinner and Hsu within the framework of the Debye approximation, but no advantages were found over the QLM model [49]. Note that lightweight or tightly bonded impurities form local modes that are above the Debye frequency and do not significantly contribute to the broadening [18].

We limit our analysis by considering the single quadratic coupling constant W. The key equations of the OSH theory, i.e., Eqs. (6), (7), and (10) and similar equations of the RM model, are strictly valid for a cubic lattice. Although the applicability of the RM model to amorphous solids can be questioned, the success of modeling the boson peak by considering a cubic lattice with randomized coupling to the nearest neighbor [50] and the similarity of the DOS measured in crystalline and disordered phases of ethanol [51] suggest that such an approach is reasonable and should be tested against the experimental data. The argument that RM amplitudes die out rapidly with the distance from the associated impurity, and therefore a short-range order is essential, also supports this idea.

The vibrational Hamiltonian, perturbed by the impurity molecule, is taken in a form similar to Eqs. (6) and (7), where we have left only quadratic terms that lead to dephasing:

$$\hat{\rm H}_{0,1} = \hat{\rm H}_{\rm p} + \frac{U_{0,1}}{2}\left[\sum_k h_k(b_k^+ + b_k^-)\right]^2. \tag{20}$$

Here, $\hat{\rm H}_{\rm p}$ is the Hamiltonian of the host matrix with unperturbed normal modes, while the second term describes the perturbation introduced by the chromophore in different electronic states with the corresponding quadratic coupling constants U_0 and $U_1 \equiv U_0 + W$. The perturbation is also quadratic in single collective coordinate $\varphi = \sum_k h_k(b_k^+ + b_k^-)$

(see also Ref. [49]) and expressions for the phonon functions $\Gamma_{0,1}$ are similar to Eqs. (12) and (13):

$$\Gamma_{0,1}(\omega) = \frac{\Gamma_{\rm p}(\omega)}{[1 - U_{0,1}\Omega_{\rm p}(\omega)]^2 + [U_{0,1}\Gamma_{\rm p}(\omega)]^2}, \tag{21}$$

where

$$\Omega_{\rm p}(\omega) = \frac{2}{\pi}\int_0^\infty \frac{\nu\Gamma_{\rm p}(\nu)}{\omega^2 - \nu^2}d\nu. \tag{22}$$

In the case $U_0 = 0$, $\Gamma_0 = \Gamma_{\rm p}$ and Eqs. (21) and (22) reduce to Eqs. (12) and (13), respectively.

Expression for $\Gamma_{\rm p}(\omega)$ can be obtained using experimental DOS $D(\omega)$ measured, for example, in neutron scattering (see Sec. IV D). Equation (10) and the equality $D(\omega) = \sum_k \delta(\omega - \omega_k)$ reveal that $\Gamma(\omega) \propto \pi[h(\omega)]^2 D(\omega)$. Using Eq. (11) as the normalization condition for $\Gamma(\omega)$, one can relate $\Gamma(\omega)$ to $D(\omega)$ as follows:

$$\Gamma(\omega) = \frac{\pi[h(\omega)]^2 D(\omega)}{\int_0^\infty \omega[h(\omega)]^2 D(\omega)d\omega}. \tag{23}$$

The frequency-dependent function $h(\omega)$ can be strictly derived by considering microscopic configuration of the atoms surrounding the impiutiry. In the long-wavelength approximation, one can take $h(\omega) \propto \sqrt{\omega}$ which results [49] from the dispersion relation of acoustic modes $\omega = v_s|\boldsymbol{k}|$, where v_s is the speed of sound and $\boldsymbol{k}$ is the wave vector [52]. An alternative scaling where $h(\omega) \propto 1/\sqrt{\omega}$, which follows from the amplitude factor, was proposed earlier for relatively high-frequency modes in amorphous solids when the long-wave approximation is no longer applicable [53]. In the previous section, we implicitly assumed a similar dependence of $h(\omega)$ when introducing a QLM according to Eq. (15). Considering a large number of sufficiently narrow QLMs distributed over frequencies according to $D(\omega)$, we also obtain $h(\omega) \propto 1/\sqrt{\omega}$.

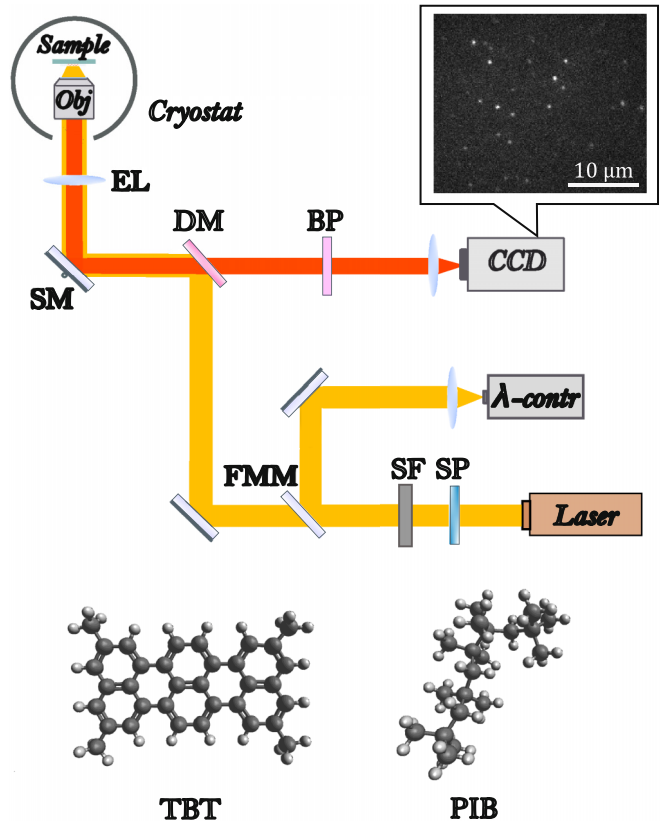

FIG. 1. Schematic diagram of the experimental setup. SP: short-pass filter; SF: spatial filter; FMM: flip-mount mirror; DM: dichroic mirror; SP: short-pass filter; BP: bandpass filter; SM: scanning mirror; EL: epilens; "λ-contr" is a portable spectrometer for laser wavelength control. The highlighted fluorescence image is recorded at 15 K at an excitation wavelength of 582.24 nm. At the bottom are the structural formulas of the compounds being studied.

III. EXPERIMENT

In our experiments we use cryogenic fluorescence-excitation spectroscopy to measure spectrally and spatially resolved ZPLs of TBT SMs embedded into thin polymer films prepared by spin-coating technique. The experimental setup uses wide-field epi-illumination as shown in Fig. 1. During the experiments, the tunable laser is focused in a spot of ~30 × 30 (120 × 120) µm^2 and its frequency is scanned over the spectral range in which the tested SMs, randomly distributed in the illuminated area, are resonantly excited, each at a different wavelength. Simultaneously, the charge-coupled device (CCD) camera collects the integral signal of the red-shifted fluorescence. After scanning, the sequence of CCD frames is processed with in-house software to recognize the fluorescent images of SMs with nanometer spatial resolution and extract their fluorescence-excitation spectra (see details in Ref. [35]).

Two experimental setups with different spectral resolution and scan range are used. The first one contains a tunable broadband (8.3 GHz or ≈ 0.3 cm^{-1}) cw dye laser (Coherent CR599) and provides a continuous scan range from 565 to 630 nm, whereas the second one features a tunable single-mode dye laser (Coherent CR599-21), which provides a scan range of ~2 cm^{-1} and high spectral resolution (its linewidth is 2 MHz or ≈ 6.7 × 10^{-5} cm^{-1}) required to measure narrow ZPLs at temperatures down to a few kelvin. Both setups are equipped with temperature-regulated optical 4He cryostats. The samples were placed in the focal planes of microscope objectives (Melles Griot 40× NA 0.65 and Microthek 60× NA 0.85, respectively, where NA is numerical aperture) mounted in the sample chamber. The redshifted fluorescence of the chromophores was separated with a dichroic mirror and the bandpass interference filters. Highly sensitive cooled CCD cameras (Andor iXon and Andor Luca) were used for the simultaneous recording of all molecules within the microscope field of view. The laser intensity was kept at 20 W/cm^2 for broadband excitation and in the range of 2–8 mW/cm^2 for the narrow-band excitation, providing a sufficient signal-to-noise ratio while avoiding light-induced line broadening (see Appendix B). More details on the experiment can be also found in Refs [54,55]. Details of the sample preparation procedure and spectra measurments are given in Appendix B.

IV. RESULTS AND DISCUSSION

A. Fluorescence-excitation spectra

To study the effect of electron-phonon coupling on ZPL broadening, we first measured the temperature-dependent

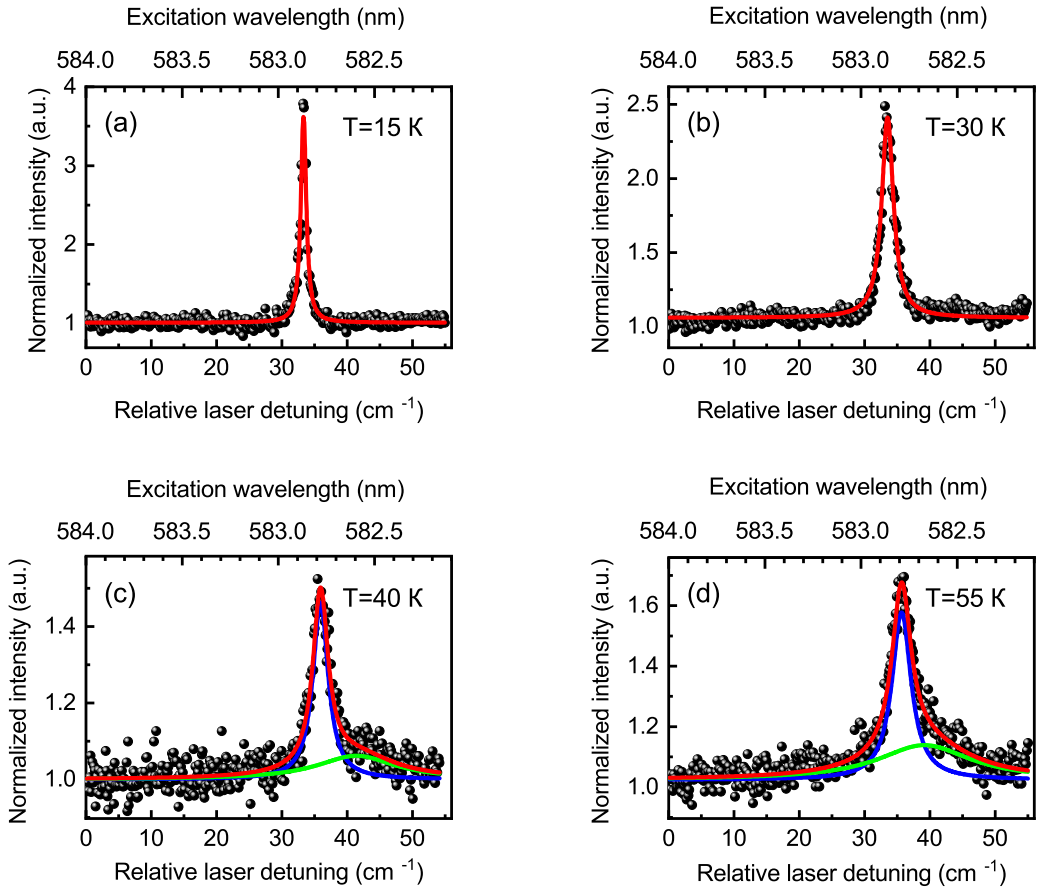

FIG. 2. Zero-phonon line in the fluorescence excitation spectrum of a single TBT molecule in PIB at 15 K (a), 30 K (b), 40 K (c), and 55 K (d). The red lines in (a) and (b) represent a Lorentzian fit with FWHM equal to 1.01 ± 0.02 and 2.17 ± 0.05 cm^{-1}, respectively. In (c) and (d), the spectral lines can be modeled as the sum of two Lorentzians. The FWHMs of the narrow components are 2.7 ± 0.2 and 3.5 ± 0.2 cm^{-1}, respectively. The acquisition time during each step of the laser scan is 0.2 s in (a), 0.5 s in (b), and 1 s in (c) and (d).

PLE spectra of TBT SMs under broadband excitation at temperatures above 15 K. The initial temperature was selected to reduce the impact of any potential contribution of the laser linewidth to the ZPL broadening. Examples of PLE spectra of the same single TBT molecule at several temperatures, revealing well-resolved ZPLs, are presented in Fig. 2.

For a reliable analysis of the homogeneous ZPL broadening, we carefully selected only those SMs whose spectra are well fitted by the Lorentzian, or by the sum of two Lorentzians if a certain asymmetry raises with temperature. We attribute this asymmetry to the manifestation of PSBs. In the present work, we paid special attention to select spectra free of visible spectral diffusion. The details of this selection are given in Appendix B. Unfortunatelly, more than 90% of the measured ZPLs had a broken shape, far from Lorentzian. Moreover, $\gamma_{\rm ph}(T)$ for them also had a zigzag shape, contradicting a general theoretical prediction of a smooth line as a result of the temperature behavior of $n(\omega)$. In addition, we measured the spectra of TBT SMs using narrow-band excitation to ensure that our results, obtained with broadband excitation, were independent of spectral resolution. The initial temperature selected in this case was 9 K, while the real upper-temperature limit in this experiment varied for different SMs due to the laser tuning-range limitation of 2 cm^{-1}.

B. Spectral diffusion

To test our assumption about the effect of SD on the spectra detected at temperatures of tens of kelvin, we measured the spectral trails for TBT SMs at a temperature of 6 K. At low temperatures the ZPL FWHM is mostly determined by the laser linewidth; thus, the spectral jumps on the order of cm^{-1} would be clearly resolved. The results are presented in Fig. 3. We observed SD in the range up to $\sim$9 cm^{-1}, which is an order of magnitude greater than the SD previously observed for TBT in PIB [56,57]. It is well known that the transition rate in TLSs increases with T according to the Boltzmann law [58]. Therefore, at temperatures in the tens of kelvin, SD can contribute to spectral line broadening, even though it is clearly resolved as spectral jumps at 6 K. Molecules exhibiting such SD were excluded from our analysis presented in Secs. IV C and IV D.

C. Analysis of the ZPL thermal broadening by considering electronic states coupled to QLMs

In the following, we focus on analyzing the ZPL temperature broadening for the three SMs. The phonon-induced contribution $\gamma_{\rm ph}(T)$ to their ZPLs is presented in Fig. 4. The first two molecules were detected using broadband excitation and carefully selected to exclude the effect of SD on their

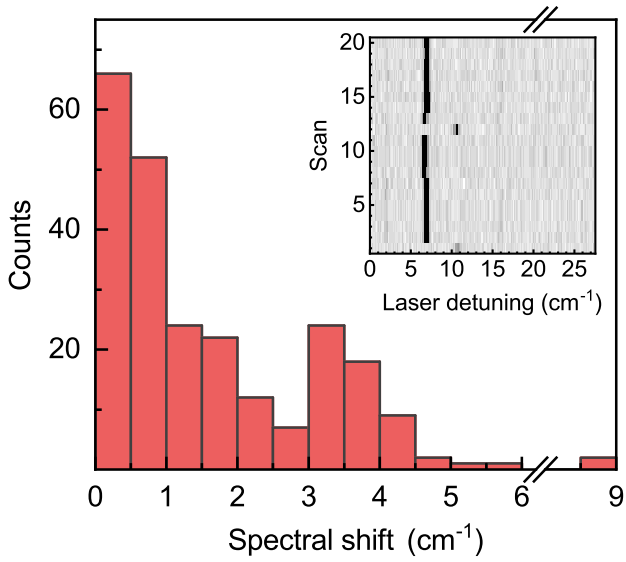

FIG. 3. Distribution of values of 240 spectral jumps measured at 6 K. The inset shows a spectral trail featuring a pronounced spectral jump of ∼4 cm^{-1}.

spectra. The procedure described in Appendix B was used to obtain the values of $\gamma_{ph}(T)$ for them. The temperature range for molecule A, whose spectra were shown in Fig. 2, was determined by the signal-to-noise ratio at which the ZPL width can be extracted. The signal from molecule B unfortunately was not observed at T above 40 K, probably due to the spontaneous spectral jump outside the laser frequency detuning range. We consider photobleaching to be much less probable due to the excellent photostability of TBT molecules. For the third SM (molecule C), the narrow-band excitation was applied, and this limited the temperature range to 22 K. We have not detected any evidence of spectral diffusion for molecule C, but it shows a wide ZPL even at relatively low temperatures.

First, we fit $\gamma_{ph}(T)$ to the weak-coupling limit using Eq. (16). We find that Eq. (16) fails to fit the data for molecule A [Fig. 4(a)]; however, it fits the data for molecule B well [Fig. 4(b)], with $\bar{\omega}$ of 41.8 ± 2.4 cm^{-1} and B of 4.0 ± 0.6 cm^{-1}, as well as for molecule C [Fig. 4(c)] with $\bar{\omega}$ of 32.1 ± 1.6 cm^{-1} and B of 10.5 ± 1.7 cm^{-1}. Since Eq. (16) is commonly used as a proof of a weak coupling to a QLM, we apply the extracted parameters to the OSH theory [Eqs. (9) and (15)]. We vary the unknown value of γ_0 within 2 tens of cm^{-1}, keeping $\omega_0 = \bar{\omega} - (B\gamma_0/8)^{1/2}$ and $W = \bar{\omega}\,(B\gamma_0/2)^{1/2}$; however, we find no satisfactory agreement between the OSH theory and the weak-coupling limit for the investigated temperature range. Nevertheless, this is not surprising since the criteria [(18a)–(18c)] are not fulfilled in these cases. The example of molecule C clearly illustrates that when γ_0 has a relatively small value of 3 cm^{-1}, inequalities (18a) and (18b) are not strictly satisfied, and no similarity between the predictions of Eq. (16) and the OSH theory is observed. For an unrealistically large $\gamma_0 = 16$ cm^{-1}, inequality (18a) is fulfilled, but (18b) is fulfilled only at temperatures up to about 15 K. At low temperatures, discrepancies occur due to violation of (18c). A similar pattern is also observed for molecule B.

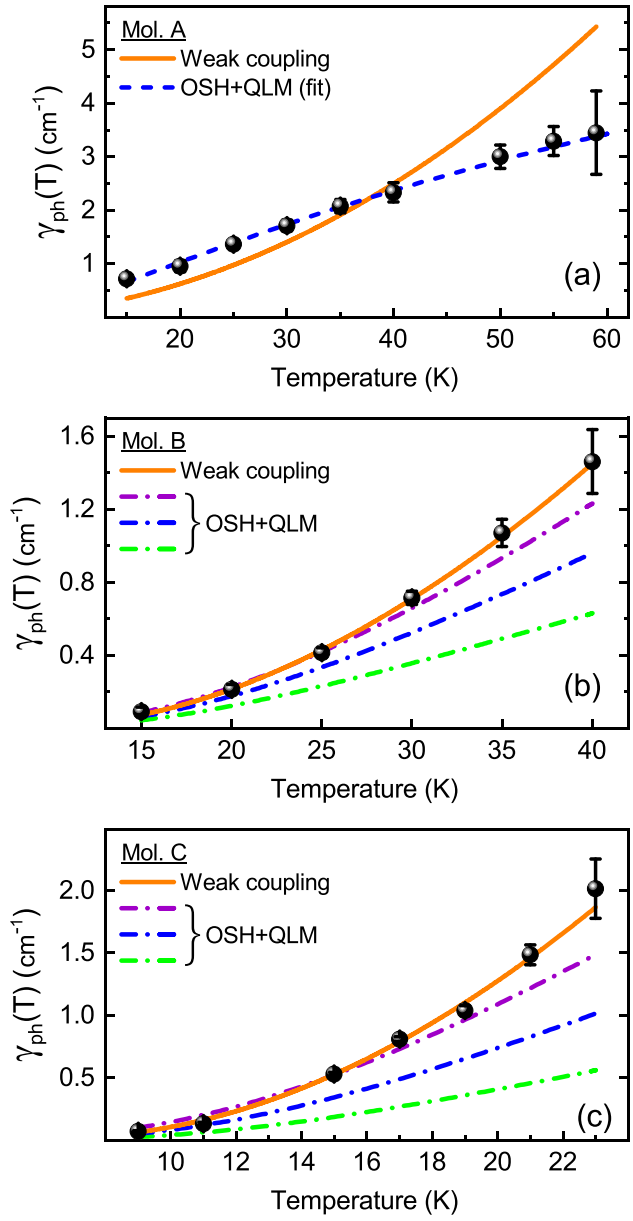

FIG. 4. Phonon-induced spectral broadening of the ZPLs of three SMs. The experimental data are represented by circles. Solid lines are the best fits to Eq. (16). The fit parameters are $\bar{\omega} = 0.09$ cm^{-1}, $B = 2.7 \times 10^{-5}$ cm^{-1} in panel (a); $\bar{\omega} = 41.8 \pm 2.4$ cm^{-1} and $B = 4.0 \pm 0.6$ cm^{-1} in panel (b); $\bar{\omega} = 32.1 \pm 3.2$ cm^{-1}, and $B = 10.5 \pm 1.7$ cm^{-1} in panel (c). The dashed-dotted lines in (b) and (c) represent the predictions of the OSH theory with $\omega_0 = \bar{\omega} - (B\gamma_0/2)^{1/2}$ and $W = \bar{\omega}\,(B\gamma_0/2)^{1/2}$ but different values of γ_0: $\gamma_0 = 3$ cm^{-1} (green line), $\gamma_0 = 8$ cm^{-1} (blue line), and $\gamma_0 = 16$ cm^{-1}, (purple line). The dashed line in (a) is a result of the fit to Eq. (9) without regard to the parameters following from the fit to Eq. (16) (see details in text). The similar fit for (b) and (c) coincides almost entirely with the solid lines and is not shown separately.

We also fit the data to Eq. (9) with $\Gamma_0(\omega)$ according to Eq. (15), unrestricted by the parameters extracted from the fit made to Eq. (16). The agreement is obtained when $\omega_0 = 5.16$ cm^{-1}, $W = 5$ cm^{-2}, and $\gamma_0 = 6.8$ cm^{-1} for molecule A; $\omega_0 = 48.4$ cm^{-1}, $W = 4700$ cm^{-2}, and $\gamma_0 = 6.2$ cm^{-1} for

molecule B; and $\omega_0 = 32\ \mathrm{cm}^{-1}$, $W = 650\ \mathrm{cm}^{-2}$, and $\gamma_0 = 14.6\ \mathrm{cm}^{-1}$ for molecule C. These parameters also do not fulfill the criteria for the transition from Eq. (9) to Eq. (16). Thus, the apperant agreement with the weak-coupling approximation is accidental. Furthermore, the obtained values appear unphysical. For example, the QLM lifetime for molecule A is shorter than one oscillation period, in which case the Lorentzian approximation to $\Gamma_{0,1}(\omega)$ is not valid. For molecule B, the saturated electron-phonon coupling is obtained [31]. The latter manifests itself in the weak dependence of $\gamma_{\mathrm{ph}}(T)$ on W that makes the spectral position of $\Gamma_1(\omega)$ undefined in principle. This phenomenon is rather a mathematical artifact of the model used, since the overlap of $\Gamma_0(\omega)$ and $\Gamma_1(\omega)$ of a Lorentzian type does not reach zero at any values of ω_0 and ω_1. Based on Eq. (12), we note that an infinite increase in ω_1 implies an infinite increase in the force constant between the chromophore and its surroundings, which is unrealistic for dispersion interactions between nonpolar molecules. The above conclusions are also valid for molecule C. We also note that the accuracy of the OSH theory becomes controversial when such a strong coupling with the QLM takes place [22].

The contradictions found between the predictions of the OSH theory and the weak-coupling limit motivated us to search for necessary conditions for an agreement between Eqs. (9) and (16). We introduce the ratio $\alpha(T) \equiv \gamma_{\mathrm{ph}}^{(\mathrm{weak})}(T)/\gamma_{\mathrm{ph}}^{(\mathrm{OSH})}(T)$ to estimate this agreement quantitatively. The "weak" index here corresponds to Eq. (16), while the "OSH" corresponds to calculations with Eq. (9) using $\Gamma_0(\omega)$ according to Eq. (15). The values obtained for molecule B ($\bar{\omega} = 42\ \mathrm{cm}^{-1}$ and $B = 4\ \mathrm{cm}^{-1}$) were employed, as well as a small B of $0.1\ \mathrm{cm}^{-1}$, which is an order of magnitude smaller than the previously reported value for the same $\bar{\omega}$ for TBT in PIB [59]. Furthermore, we varied the value of γ_0 over a wide range while keeping $W = \bar{\omega}(B\gamma_0/2)^{1/2}$.

These two examples are shown in Fig. 5. For $B = 0.1\ \mathrm{cm}^{-1}$, $\alpha(T)$ deviates from unity at high temperatures because $\gamma_{\mathrm{ph}}(T)$ increases and eventually violates inequality (18c), and at low temperatures when condition (18b) is not met. An agreement is observed only for intermediate γ_0 within a relatively narrow temperature range. Note that for small values of γ_0, $\alpha(T)$ flattens at a value slightly larger than unity, since inequality (18a) is not strictly satisfied. The case shown in Fig. 5(b) is for a more realistic value of $B = 4\ \mathrm{cm}^{-1}$, corresponding to molecule B. It reveals a dramatic deviation of $\alpha(T)$ from unity at practically any temperature.

Although we have only considered a QLM with a frequency of $42\ \mathrm{cm}^{-1}$, our conclusions can be extended for other energy modes of PIB. From Ref. [59] one can estimate the available $\bar{\omega}$ range from a few cm^{-1} to $\sim 80\ \mathrm{cm}^{-1}$, with $B \approx \eta\omega^{2.6}$, where η is in the range of $\sim 2 \times 10^{-4}$ to $\sim 20 \times 10^{-4}$. It is easy to show that for such $B(\omega)$ it is impossible to fulfill (18a) and (18b) and justify the transition to Eq. (16).

Summarizing, we conclude that an apparent agreement between the data and the weak-coupling limit predictions does not prove a real weak coupling with a single QLM (as has been previously assumed [26,27,60,61]). The evidence based on the agreement between the experimental data and Eq. (16) is illusive, and the generally accepted approach to the ZPL broadening based on perturbative expressions should be reconsidered. Remarkably, these findings could be extended to a larger number of dye-doped glasses. For example, in Ref. [25] photon echo measurements were performed for seven doped amorphous systems, and for all of them the agreement with the weak-coupling limit was obtained with parameters of the same order as for TBT in PIB. Therefore, the conclusion obtained for TBT in PIB should also be valid for the systems investigated in Ref. [25].

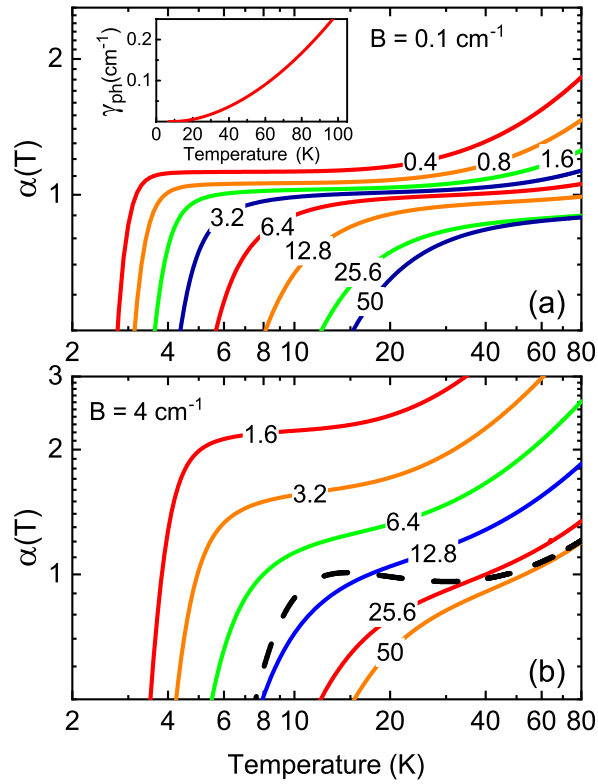

FIG. 5. The ratio $\alpha(T) \equiv \gamma_{\mathrm{ph}}^{(\mathrm{weak})}(T)/\gamma_{\mathrm{ph}}^{(\mathrm{OSH})}(T)$ for the SM-QLM coupling. For all solid lines, $\bar{\omega} = 42\ \mathrm{cm}^{-1}$ and $W = \bar{\omega}\,(B\gamma_0/2)^{1/2}$. The variable value of γ_0 in cm^{-1} labels the corresponding curve. Panel (a) shows $\alpha(T)$ when $B = 0.1\ \mathrm{cm}^{-1}$. The inset shows theoretical results for $\gamma_{\mathrm{ph}}(T)$ as predicted by Eq. (16). The solid lines in panel (b) are obtained for $B = 4\ \mathrm{cm}^{-1}$. The dashed line is obtained using Eqs. (9) and (15), where $W = 4700\ \mathrm{cm}^{-2}$, $\omega_0 = 48\ \mathrm{cm}^{-1}$, and $\gamma_0 = 6.2\ \mathrm{cm}^{-1}$.

D. Analysis of the ZPL temperature broadening in the framework of the RM model

To calculate the spectrum of RMs, we begin with the DOS for pure PIB $D_{\mathrm{PIB}}(\omega)$, obtained in independent neutron-scattering experiments [62] and shown in Fig. 6. The inset shows $D_{\mathrm{PIB}}(\omega)/\omega^2$ to highlight the boson peak. Only acoustic-like modes with energies below 20 meV ($\sim 160\ \mathrm{cm}^{-1}$) are considered, which are mainly attributed to interchain vibrations, similar to the approach taken in Refs. [63,64] with polyethylene and several normal alkanes. The DOS was fitted with a polynomial $\sum_{i=1}^{7} A_i\omega^i$ to ensure a good agreement with the experimental data. To avoid artifacts in further calculations two conditions were imposed: $D_{\mathrm{PIB}}(0) = 0$ and $D_{\mathrm{PIB}}(\omega) > 0$.

The shape of $\Gamma_{\mathrm{PIB}}(\omega)$ for pure PIB strongly depends on coefficients $h(\omega)$. We start our calculations by considering

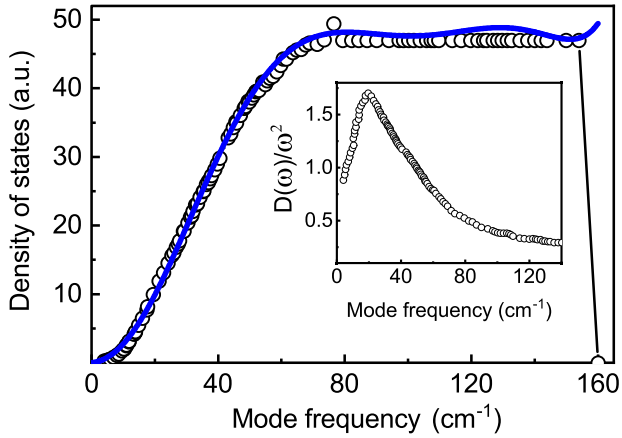

FIG. 6. The DOS of pure PIB $D_{\mathrm{PIB}}(\omega)$ obtained in the independent neutron-scattering experiments [62] (circles). The solid line is the fit result. The inset shows $D_{\mathrm{PIB}}(\omega)/\omega^2$.

PIB normal modes of the propagating character within the long-wavelength approximation, which implies $h(\omega) \propto \sqrt{\omega}$. In this case, $\Gamma_{\mathrm{PIB}}(\omega)$ is expressed through $D_{\mathrm{PIB}}(\omega)$ as follows:

$$\Gamma_{\mathrm{PIB}}(\omega) = \frac{\pi \omega D_{\mathrm{PIB}}(\omega)}{\int_0^\infty \omega^2 D_{\mathrm{PIB}}(\omega) d\omega}. \tag{24}$$

The rise of resonant modes in PIB as per Eq. (21) at various $U_{0,1}$ values is shown in Fig. 7. The value of $U_{0,1} = 0$ corresponds to the unperturbed normal modes of PIB. Negative values of $U_{0,1}$ characterize the decrease of the quadratic coupling constant, which leads to the appearance of RMs. Note that parameters $U_{0,1}$ are relative and have the meaning of bond weakening compared to PIB interchain bonds. As the modulus of $U_{0,1}$ increases, the maximum of $\Gamma_{0,1}(\omega)$ becomes clearly visible in the spectrum and moves nonlinearly into the low-frequency region. When it reaches a relatively small but nonzero frequency of ≈ 0.26 cm^{-1} at $U_{0,1}^{\max} \approx -5355$ cm^{-2}, the absolute value of the force constant approaches zero, i.e.,

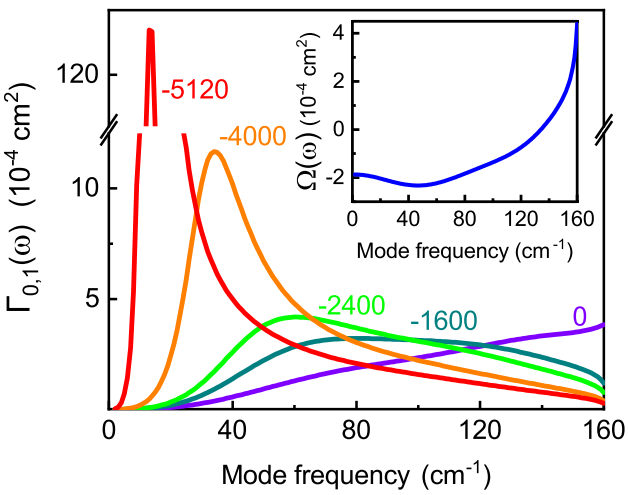

FIG. 7. The shape of $\Gamma_{0,1}(\omega)$ for various values of the coupling constant $U_{0,1}$ (each curve is labeled with its corresponding value). The inset shows $\Omega_{\mathrm{p}}(\omega)$ calculated according to Eq. (22).

the bond is broken and the impurity molecule no longer responds to its surroundings [32].

Figure 8 displays the ZPL thermal broadening against the RM model fit for the three TBT SMs considered above. The values of $\gamma_{\mathrm{ph}}(T)$ are calculated using Eq. (9), where $\Gamma_{0,1}(\omega)$ follows from Eqs. (21) and (24). For all three molecules, the agreement with the theoretical model is good. Note a dramatically increased density of low-energy modes in all cases and that the calculated $\Gamma_{0,1}(\omega)$ are unique for each SM. For molecule A, $\Gamma_{0,1}(\omega)$ are sharply peaked with a maximum at approximately 11.0 and 12.6 cm^{-1}, respectively. Such functions are very similar in shape to the QLMs discussed above. Significantly different lambda-shaped $\Gamma_{0,1}(\omega)$ are shown in Figs. 8(b) and 8(c). They exhibit the pronounced high-frequency tails that contribute significantly to the ZPL broadening at temperatures in the tens of kelvin. It is possible to obtain the "absolute" values of the force constants $\tilde{U}_{0,1}$ as $\tilde{U}_{0,1} = U_{0,1} - U_{0,1}^{\max}$, which allows to estimate the strength of the electron-phonon coupling. For molecule A, we obtain 245 and 183 cm^{-2}, respectively. For molecule B, the values are 2795 and 1859 cm^{-2}, and for molecule C, the values are 2955 and 1059 cm^{-2}. Therefore, the first two SMs reveal the electron-phonon coupling of comparable strength, whereas molecule C exhibits stronger coupling. The differences in the strength of the electron-phonon interaction may be due to the different orientation of the SM dipole moments in the S_0 and S_1 states relative to the dipole moment of the nearest PIB molecule [65]. Spatial variations of U_0 can arise due to various factors, such as the distribution of induced dipole values [66], different distances between the TBT and PIB molecules, their various relative orientation, or the presence of permanent dipole moments in the chromophores due to the host-induced symmetry breaking [65,67].

After considering RMs as propagating waves, we examine a model in which RMs are treated as quasilocal modes when the frequency dependence $h(\omega) \propto 1/\sqrt{\omega}$ is proportional to the mode amplitude [53]. This frequency dependence is similar to that of the QLM model discussed earlier. However, here we actually consider a wide spectrum of QLMs distributed according to $D_{\mathrm{PIB}}(\omega)$. From $h(\omega) \propto 1/\sqrt{\omega}$ it follows that $\Gamma_{\mathrm{PIB}}(\omega) \sim (1/\omega) D_{\mathrm{PIB}}(\omega)$. To satisfy $\Gamma_{\mathrm{PIB}}(0) = 0$, we set the coefficient A_1 in the polynomial for $D_{\mathrm{PIB}}(\omega)$ equal to zero, since it has virtually no effect on the shape of $D_{\mathrm{PIB}}(\omega)$. We also use a normalization condition according to Eq. (23).

Calculations show that in this case the RM model predicts a quasilinear ZPL broadening for all values of $U_{0,1}$. Therefore, it is completely unable to explain the observed dephasing for molecules B and C. The predictions of this model for $U_0 = 0$ [i.e., $\Gamma_0(\omega) = \Gamma_{\mathrm{PIB}}(\omega)$] and two values of U_1, which provide $\gamma_{\mathrm{ph}}(T)$ comparable to the experimental values for low and high temperatures, are shown in Fig. 9 together with the data for molecule B. Using a zero value of U_0 is a reasonable strategy to maximize the density of high-energy modes and thus provide the necessary temperature rise in $\gamma_{\mathrm{ph}}(T)$. However, even this strategy does not lead to a match between the experimental data and the theoretical predictions. The observed discrepancy is due to the excessively large values of $\Gamma_{\mathrm{PIB}}(\omega)$ for small ω (see inset in Fig. 9), which, when multiplied by $n(\omega)[n(\omega)+1]$ according to Eq. (9), lead to significant broadening already at relatively low temperatures.

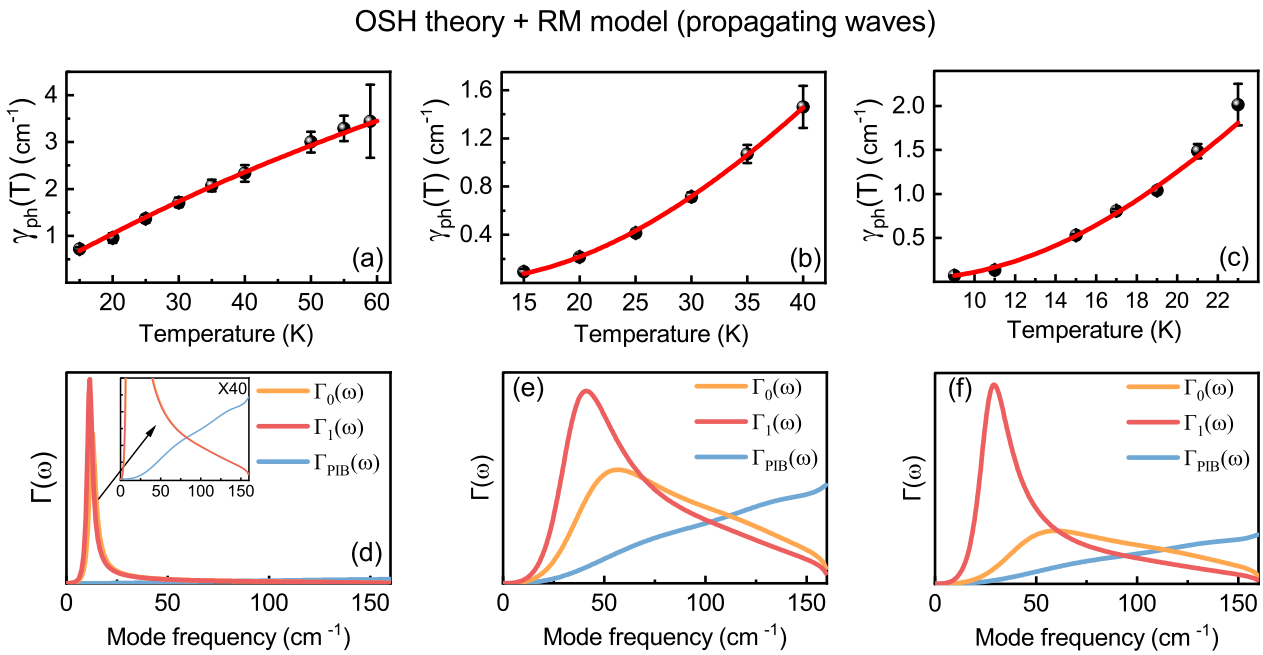

FIG. 8. Thermal broadening of ZPLs in the framework of the RM model for propagating phonons. Panels (a)–(c) show the same data as in Fig. 4 and calculations of $\gamma_{\rm ph}(T)$ using the OSH theory with the RM model. The values of U_0 and U_1 are -5110 and -5172 cm^{-2} (a), -2560 and -3496 cm^{-2} (b), and -2400 and -4256 cm^{-2} (c), respectively. Panels (d)–(f) show the corresponding $\Gamma_{\rm PIB}(\omega)$ for pure PIB (blue line) and $\Gamma_{0,1}(\omega)$ (orange and red lines).

E. Opportunities and prospects of the RM model

Our results suggest that single-molecule spectroscopy can be applied to analyze $h(\omega)$ in amorphous media, which is of undoubted interest. On the one hand, $h(\omega)$ can hypothetically contain a crossover between propagating phonons and, e.g., molecular cluster vibrations [68] or strongly scattered modes [69]. On the other hand, the opportunity to test a model with a fluctuating wave vector is also intriguing [70]. Although it is impossible to unambiguously determine $\Gamma_{0,1}(\omega)$ by analyzing only $\gamma_{\rm ph}(T)$, $\Gamma_{0,1}(\omega)$ can be extracted from PSB in luminescence and luminescence excitation spectra, respectively [44]. The one-phonon function $v^1_{0,1}(\omega)$, which defines the probability of one-phonon transitions, is approximately proportional to $\omega\xi(\omega)\Gamma_{0,1}(\omega)$ at a moderate strength of the linear electron-phonon coupling $\xi(\omega)$ [31]. The RM model also provides a qualitative explanation for the fluctuating electron-phonon interaction strength [71,72]. Both spatial and temporal changes in the local $\Gamma_{0,1}(\omega)$ will affect the ZPL width and the PSB shape, as well as the Huang-Rhys factor [31].

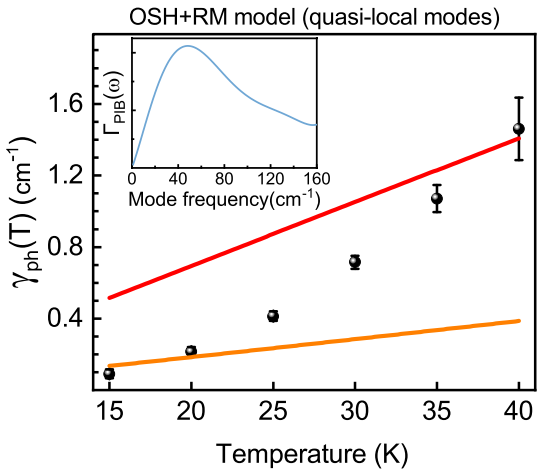

FIG. 9. Thermal broadening of the ZPL of molecule B in comparison with the predictions of the RM model for quasilocal phonons. The orange line ($U_0 = 0$, and $U_1 = -320$ cm^{-1}) and the red one ($U_0 = 0$, and $U_1 = -768$ cm^{-1}) are examples of the linear broadening law, which is typical for all values of $U_{0,1}$.The inset shows $\Gamma_{\rm PIB}(\omega)$. The spectral phonon functions $\Gamma_0(\omega)$ are equal to $\Gamma_{\rm PIB}(\omega)$ for both curves, and both $\Gamma_1(\omega)$ are practically indistinguishable from it.

An interesting scenario occurs when $U_{0,1} > 0$, indicating the presence of light impurities or strong bonds. In this case, the density of phonons in the acoustic continuum decreases in favor of high-energy local modes, and the theory predicts a decrease in phonon-induced broadening. This conclusion appears counterintuitive, since one would expect that weaker coupling to the matrix should result in narrower ZPLs. However, this alternative approach may be far more promising. Modifying of the local vibrational dynamics of solids through the parameters of the electron-phonon coupling has a great potential for developing efficient photonic devices with desired characteristics that operate at high (room) temperatures. A somewhat similar approach has recently been demonstrated for spin coherence prolongation in diamonds [73].

By comparing existing microscopic models describing the temperature behavior of pure optical dephasing, we conclude that the RM model can be considered as the most general one. In addition to the weak-coupling limit represented by Eq. (16), certain related formulas are also used in the processing of experimental data for various emitters, not only organic molecules [4,5,24,74]. In particular, the Arrhenius

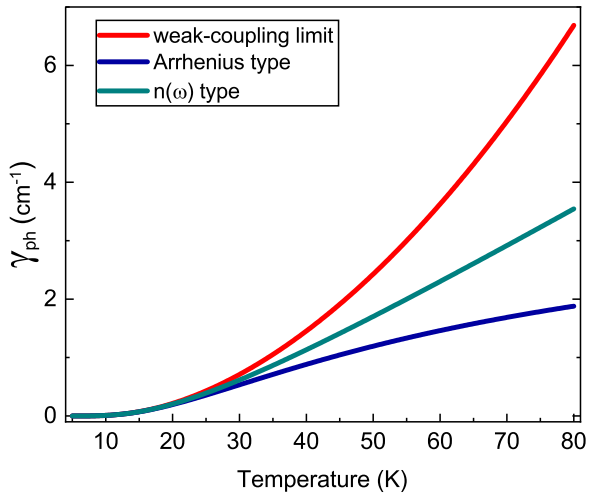

FIG. 10. Comparison of different broadening laws of the ZPL due to a weak coupling to a single vibrational mode (see details in the text). Here, $\bar{\omega} = 42$ cm^{-1} and $B = 4$ cm^{-1}.

type of broadening $\gamma_{ph}(T) \sim \exp[-\hbar\bar{\omega}/(kT)]$ is quite common. It can be easily derived from Eq. (16), assuming $kT \ll \hbar\omega$. Similarly, the condition $kT \gg \hbar\omega$ leads to a somewhat different law, $\gamma_{ph}(T) \sim n(\bar{\omega})$. In Fig. 10, we compare these broadening laws and find that they are within 10% accuracy, while $kT \lesssim \hbar\bar{\omega}/3$. Therefore, it is possible to extend our considerations to these broadening laws, at least in the indicated temperature range, starting from the vibrational dynamics of the studied solid-state emitter, especially if it can be obtained by quantum-chemical calculations [75,76].

Within the RM model it is also easy to obtain the classical McCumber-Sturge formula [15]. Assuming that the impurity has no appreciable influence on the host normal modes, then in the framework of the Debye approximation $\Gamma_0(\omega) = (5\pi/{\omega_D}^5)\omega^3$, where ω_D is the Debye frequency. The identity of $\Gamma_0(\omega)$ and $\Gamma_1(\omega)$ is true if $W/{\omega_D}^2 \ll 1$ and then Eq. (9) reduces to the well-known expression

$$\gamma_{ph}(T) = A\left(\frac{kT}{\omega_D}\right)^7 \int_0^{\omega_D/kT} \frac{x^6 dx}{\sinh^2(x/2)}, \qquad (25)$$

where A is a constant.

It should be noted that the pure dephasing considered in this paper is not the only possible reason for the ZPL temperature broadening of solid-state emitters. Dephasing processes involving population transfer between electronic states can be dominant, in which case the two-level emitter approximation is no longer applicable. Examples include paramagnetic rare-earth doped materials [77] and NV or SiV color centers in diamonds [2,3]. The presence of multiple competing channels obviously complicates the dephasing pattern.

V. CONCLUSIONS

In summary, we have revised the problem of phonon-induced ZPL broadening for SMs embedded in amorphous solids. We have measured the ZPLs of TBT SMs in a PIB matrix over a wide temperature (9–60 K) and spectral (up to 56-cm^{-1}) range and applied theoretical analysis based on the nonperturbative theory of electron-phonon coupling developed by Osad'ko, Skinner, and Hsu. We have found that the expression widely used to describe a weak coupling between a SM and a QLM, obtained by perturbation theory, is inconsistent with the nonperturbative approach in almost all circumstances. Although we have experimentally observed ZPL broadening proportional to $\exp(-\hbar\bar{\omega}/kT)/[\exp(-\hbar\bar{\omega}/kT) - 1]^2$, which is commonly associated with a weak coupling to a single QLM, we show that this agreement is accidental. The widely used concept of QLMs cannot explain our experimental results even in the case of electron-phonon coupling of arbitrary strength. Instead, we interpret our data in terms of RMs in the long-wavelength approximation. These modes result from a significant change in the vibrational DOS of the host matrix due to the changes in the forces acting on the nearest neighborhood around an impurity. We show that the vibrational spectrum of the RMs for a particular material can be obtained from the data on the DOS. We also test the model considering the RMs arising from the PIB normal modes of a quasilocal character and find it incompatible with the observed dephasing. We suggest that the approach presented in this paper can be applicable to other solid-state emitters, and encourage a critical look at the origins of spectral line broadening published in the literature.

ACKNOWLEDGMENTS

The work was carried out with the financial support from the Ministry of Education of the Russian Federation within the framework of the state assignment of the Moscow Pedagogical State University "Physics of nanostructured materials and highly sensitive sensors: synthesis, fundamental research and applications in photonics, life sciences, quantum and nanotechnologies" (A.V.N.). A.O.S., I.Yu.E., and A.V.N are members of the Leading Scientific School of the Russian Federation, supported by President of the Russian Federation, Grant No. NSh-776.2022.1.2. TBT was synthesized at the Max-Planck-Institute for Polymer Research, Mainz, Germany and kindly provided by Th. Basché.

APPENDIX A: DERIVATION OF EQ. (17c)

To take $n(\omega)[n(\omega) + 1]$ out of the integral [Eq. (9)], we require that $\Delta\{n(\omega)[n(\omega) + 1]\}$, the change in $n(\omega)[n(\omega) + 1]$, be much smaller than the value of $n(\omega)[n(\omega) + 1]$ itself within the range where the value of $\Gamma_0(\omega)\Gamma_1(\omega)$ contributes most significantly to the integral. The change in $\Delta\{n(\omega)[n(\omega) + 1]\}$ can be estimated using the Taylor series at $\bar{\omega}$, for which we can restrict ourselves to calculating the first two derivatives. Assuming for simplicity that $\hbar = k = 1$, one can obtain the first derivative:

$$\begin{aligned}\frac{d\{n(\omega)[n(\omega)+1]\}}{d\omega} &= \frac{1}{T}\frac{\exp(\omega/T)[\exp(\omega/T)-1] - 2\exp(2\omega/T)}{[\exp(\omega/T)-1]^3} \\ &= \frac{n(\omega)[n(\omega)+1]}{T}\frac{\exp(\omega/T)+1}{\exp(\omega/T)-1}. \end{aligned} \qquad (A1)$$

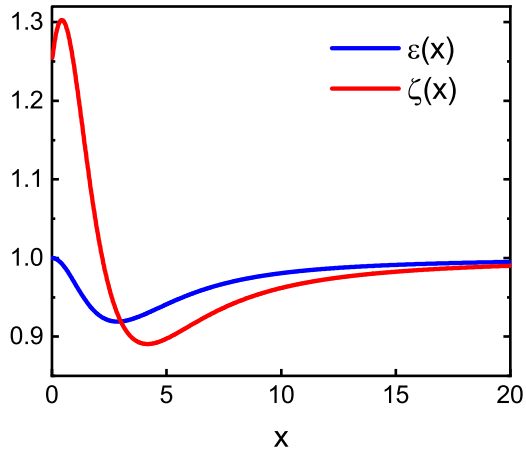

FIG. 11. A graphical comparison of the right-hand sides of Eqs. (A1) and (A2) by plotting their ratio $\varepsilon(x) = \{x[\exp(x)+1]\}/\{\sqrt{4+x^2}[\exp(x)-1]\}$ (blue line) as well as a comparison of Eqs. (A3) and (A4) by plotting their ratio $\zeta(x) = \{x^2\exp(x)[\exp(x)+4]\}/\{(x^2+4)[\exp(x)-1]^2\}$ (red line), where $x = \omega/T$.

With 10% accuracy (see Fig. 11), this can be written as follows:

$$\frac{d\{n(\omega)[n(\omega)+1]\}}{d\omega} \approx n(\omega)[n(\omega)+1]\left(\frac{4}{\omega^2}+\frac{1}{T^2}\right)^{1/2}. \tag{A2}$$

For the second derivative, one gets

$$\begin{aligned}\frac{d^2\{n(\omega)[n(\omega)+1]\}}{d\omega^2} &= \frac{\exp(\omega/T)[\exp(2\omega/T)+4\exp(\omega/T)+1]}{T^2[\exp(\omega/T)-1]^4} \\ &\approx \frac{\{n(\omega)[n(\omega)+1]\}^2}{T^2}[\exp(\omega/T)+4].\end{aligned} \tag{A3}$$

With 30% accuracy (see Fig. 11), this can be written as follows:

$$\frac{d^2\{n(\omega)[n(\omega)+1]\}}{d\omega^2} \approx n(\omega)[n(\omega)+1]\left(\frac{4}{\omega^2}+\frac{1}{T^2}\right). \tag{A4}$$

Therefore,

$$\begin{aligned}&\Delta\{n(\omega)[n(\omega)+1]\} \\ &\quad\approx n(\omega)[n(\omega)+1]|_{\omega=\bar\omega} \\ &\quad\times\left[1+\left(4+\frac{\bar\omega^2}{T^2}\right)^{1/2}\frac{\omega-\bar\omega}{\bar\omega}+\frac{1}{2}\left(4+\frac{\bar\omega^2}{T^2}\right)\left(\frac{\omega-\bar\omega}{\bar\omega}\right)^2\right].\end{aligned} \tag{A5}$$

If $\Gamma_0(\omega)\Gamma_1(\omega)$ is symmetric about the point $\omega = \bar\omega$, then the linear term makes no contribution to the integral and the first term to consider is the quadratic term. Thus, one gets the condition for taking $n(\omega)[n(\omega)+1]$ out of the integral as follows:

$$\frac{\Delta\{n(\omega)[n(\omega)+1]\}}{n(\omega)[n(\omega)+1]} \approx \frac{1}{2}\left(4+\frac{\bar\omega^2}{T^2}\right)\left(\frac{\omega-\bar\omega}{\bar\omega}\right)^2 \ll 1. \tag{A6}$$

As stated above, this inequality should hold in the range of ω where $\Gamma_0(\omega)\Gamma_1(\omega)$ contributes most to the integral in Eq. (9). This interval can be estimated as $|\omega-\bar\omega| \leqslant \Delta\omega$ if the locations of the maxima for $\Gamma_0(\omega)$ and $\Gamma_1(\omega)$ are close to each other. If the two maxima are split, then the validity interval for ω should also include the splitting. Therefore, the estimate $|\omega-\bar\omega| \leqslant \Delta\omega$ is the most conservative. Hence, Eq. (17c) in the main text follows.

APPENDIX B: METHODS

1. Sample preparation

The samples were thin polymer films doped with impurity TBT molecules prepared via spin-coating technique on a glass substrate. PIB (molecular weight of 420 000 g/mol, Aldrich) was dissolved in toluene at a concentration of ∼50 mg/mL. TBT was also dissolved in toluene (Aldrich) at an initial concentration of about 10^{-6} mol/L. The resulting solutions were thoroughly mixed in a ratio of 1:10, after which a small drop of the mixture (3–4 μL) was applied to a glass substrate rotating at a speed of 1700–1800 rpm. The sample was rotated at this speed for 30 s, and then the speed was gradually increased to 3000 rpm; the sample was rotated for another 30 s and then was placed in a vacuum oven, where it was kept for 2 h at a temperature of 373 K and a pressure of ∼1 kPa to remove the residual solvent. To find the concentration of TBT molecules, required for robust single-molecule detection, the solution of molecules in toluene was successively diluted until within 15–20 SMs could be observed simultaneously in the field of view of the microscope (∼30 × 30 μm^2 and 120 × 120 μm^2 for two setups, respectively). Such a concentration results in a typical minimum distance of at least 1 μm between the two closest luminescent SMs (see Fig. 1).

2. Temperature-dependent fluorescence-excitation spectroscopy

The experimental setup is shown in Fig. 1. During the measurements, the sample was cooled by a flow of helium. The sample temperature is controlled using a dual-circuit control system by varying the flow of helium gas and a resistive

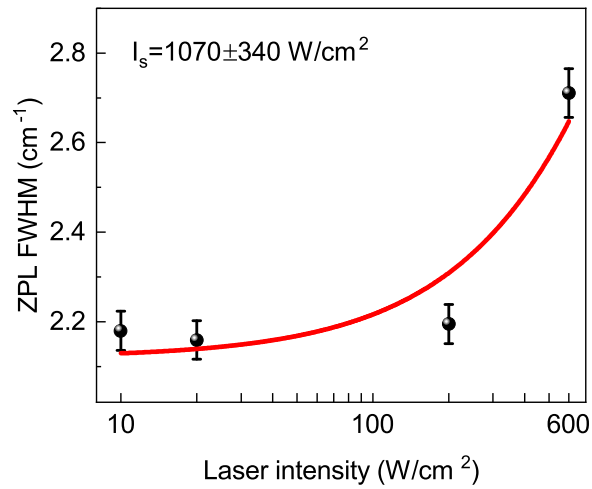

FIG. 12. Linewidths of molecule A at 30 K for different excitation laser intensities.

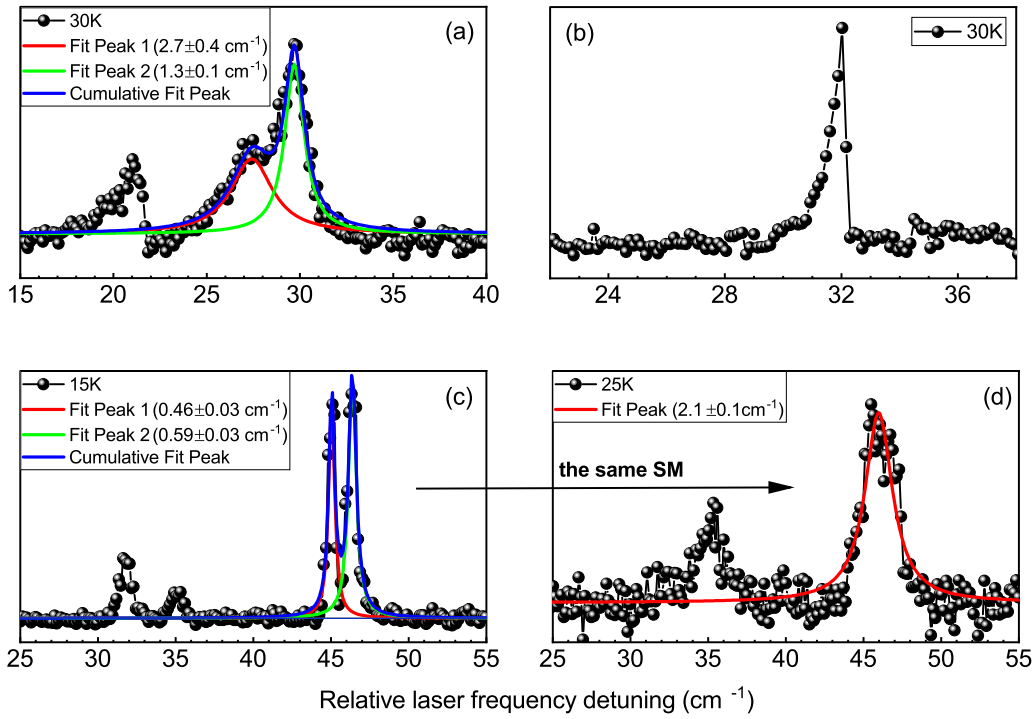

FIG. 13. The examples of rejected SM spectra. In panel (a) there is a spectrum consisting of at least two ZPLs with different widths. In panel (b) the effect of line-motion narrowing is shown. In (c) and (d) two initially separated spectral lines become unresolved with increasing temperature.

heater. The system rested for 5 min at each temperature to achieve thermal equilibrium in the sample.

By means of a broadband laser, TBT molecules were excited from the very edge of the long-wavelength wing of the absorption spectrum [78]: from 584 to ≈582.1 nm. We have previously examined this spectral range and found no features in the SM spectra that distinguish it from the range of maximum absorption [79]. At a laser intensity of 20 W/cm^2, we find no signature of light-induced spectral line broadening. An intensity-dependent linewidth of molecule A at 30 K is given in Fig. 12. Although the measured dependence on laser intensity I can be satisfactorily fitted by the well-known equation $\gamma(I) = \gamma_{I\to 0}\sqrt{1 + I/I_S}$ [80], with a saturation intensity I_S of 1070 ± 340 W/cm^2, we found no correlation between fluorescence intensity and laser power. We conclude that the observed dependence is probably due to light-induced spectral diffusion. The narrowband excitation was used to investigate the 567 – 577 nm range, which is very close to the absorption maximum. The excitation power was kept at 2–8 mW/cm^2. To block scattered laser light from the detection channel for both setups, we used a combination of a dichroic mirror that transmits radiation with a wavelength above 605 nm and a bandpass filter that transmits light from 612 to 644 nm, where the vibronic band of TBT is detected.

3. Spectra analysis

Since the ZPL shape corresponds to the Voigt profile, we used computer simulation of the spectrum to determine the homogeneous linewidth $\gamma_{\mathrm{ZPL}}(T)$. The contour of the spectral line $S(\omega_{\mathrm{las}}, T)$ measured in the experiment was modeled as a convolution of the Gaussian laser profile and the Lorentzian ZPL shape, with integration replaced by summation to simplify the calculations:

$$S(\omega_{\mathrm{las}}, T) = \sum_{\omega} \frac{2\sqrt{\ln 2}}{\pi\sqrt{\pi}\gamma_{\mathrm{las}}} \exp\left[4\ln 2\left(\frac{\omega - \omega_{\mathrm{las}}}{\gamma_{\mathrm{las}}}\right)^2\right] \times \left\{\frac{\gamma_{\mathrm{ZPL}}(T)/2}{(\omega - \omega_{\mathrm{ZPL}})^2 + [\gamma_{\mathrm{ZPL}}(T)/2]^2}\right\}, \quad \text{(A7)}$$

where ω_{las} is the laser frequency, γ_{las} is the laser linewidth, $\gamma_{\mathrm{ZPL}}(T)$ is the desired ZPL linewidth according to Eq. (3), and ω_{ZPL} is its spectral position. The value of ω_{ZPL} was determined by fitting the measured spectra with a simple Lorentzian profile. The FWHM of the Lorentz profile was also determined for each spectrum. Furthermore, we varied the value of $\gamma_{\mathrm{ZPL}}(T)$ in Eq. (A7) and fitted the calculated spectra to a Lorentzian contour. The true value of $\gamma_{\mathrm{ZPL}}(T)$ was determined as that for which the fitting results were the same with sufficient accuracy. As shown in Sec. II, $\gamma_{\mathrm{ZPL}}(T)$ was determined by three contributions [Eq. (3)]. We calculated the phonon-induced contribution to the linewidth as $\gamma_{\mathrm{ph}}(T) = \gamma_{\mathrm{ZPL}}(T) - bT^a$, where b and a equal 10^{-3} cm^{-1} and 1.1, respectively [41].

As discussed in Sec. IV, the detection of spectra consisting only of homogeneously broadened ZPL is challenging. We associate the complex shape of most of the observed spectra with the ZPL spectral instability due to SD during laser scanning. To obtain the most reliable data for analysis, we selected only those SMs whose spectra were closest to the bell shape and did not reveal a clear effect of spectral diffusion. To do

this, we excluded from the analysis those molecules that did not match the following criteria:

(i) The detectable spectrum should be within the temperature range of 15 to at least 40 K.
(ii) There should not be two or more closely located ZPLs in one spectrum.
(iii) The spectra should not show a clear visible splitting, except for temperatures above 40 K, where a significant difference in peak intensity is observed (see Fig. 2).
(iv) The absence of a visible complex shape of the spectra that cannot be unambiguously decomposed into several Lorentzian components.
(v) No effect of the line motion narrowing due to the ZPL resonant frequency change during the laser scan.
(vi) The extracted $\gamma_{\mathrm{ph}}(T)$ remained monotonic over the entire temperature range.

In Fig. 13 we show the typical spectra, which were excluded from our analysis.

[1] P. Tighineanu, C. L. Dreeßen, C. Flindt, P. Lodahl, and A. S. Sørensen, Phonon decoherence of quantum dots in photonic structures: Broadening of the zero-phonon line and the role of dimensionality, Phys. Rev. Lett. **120**, 257401 (2018).

[2] K.-M. C. Fu, C. Santori, P. E. Barclay, L. J. Rogers, N. B. Manson, and R. G. Beausoleil, Observation of the dynamic Jahn-Teller effect in the excited states of nitrogen-vacancy centers in diamond, Phys. Rev. Lett. **103**, 256404 (2009).

[3] K. D. Jahnke, A. Sipahigil, J. M. Binder, M. W. Doherty, M. Metsch, L. J. Rogers, N. B. Manson, M. D. Lukin, and F. Jelezko, Electron–phonon processes of the silicon-vacancy centre in diamond, New J. Phys. **17**, 043011 (2015).

[4] N. R. Jungwirth, B. Calderon, Y. Ji, M. G. Spencer, M. E. Flatté, and G. D. Fuchs, Temperature dependence of wavelength selectable zero-phonon emission from single defects in hexagonal boron nitride, Nano Lett. **16**, 6052 (2016).

[5] Y. Xue *et al.*, Single-photon emission from point defects in aluminum nitride films, J. Phys. Chem. Lett. **11**, 2689 (2020).

[6] W. E. Moerner and M. Orrit, Illuminating single molecules in condensed matter, Science **283**, 1670 (1999).

[7] X.-L. Chu, S. Götzinger, and V. Sandoghdar, A single molecule as a high-fidelity photon gun for producing intensity-squeezed light, Nat. Photonics **11**, 58 (2017).

[8] M. Colautti, F. S. Piccioli, Z. Ristanović, P. Lombardi, A. Moradi, S. Adhikari, I. Deperasinska, B. Kozankiewicz, M. Orrit, and C. Toninelli, Laser-induced frequency tuning of Fourier-limited single-molecule emitters, ACS Nano **14**, 13584 (2020).

[9] R. C. Schofield, D. P. Bogusz, R. A. Hoggarth, S. Nur, K. D. Major, and A. S. Clark, Polymer-encapsulated organic nanocrystals for single photon emission, Opt. Mater. Express **10**, 1586 (2020).

[10] C. Toninelli *et al.*, Single organic molecules for photonic quantum technologies, Nat. Mater. **20**, 1615 (2021).

[11] D. Rattenbacher, A. Shkarin, J. Renger, T. Utikal, S. Götzinger, and V. Sandoghdar, On-chip interference of scattering from two individual molecules, Optica **10**, 1595 (2023).

[12] C. Gooijer, F. Ariese, and J. W. Hofstraat, *Shpol'skii Spectroscopy and Other Site-Selection Methods: Applications in Environmental Analysis, Bioanalytical Chemistry, and Chemical Physics*, Chemical Analysis (John Wiley & Sons, Hoboken, NJ, 2000).

[13] W. P. Ambrose and W. E. Moerner, Fluorescence spectroscopy and spectral diffusion of single impurity molecules in a crystal, Nature (London) **349**, 225 (1991).

[14] R. Kettner, J. Tittel, Th. Basche, and C. Braeuchle, Optical spectroscopy and spectral diffusion of single dye molecules in amorphous spin-coated polymer films, J. Phys. Chem. **98**, 6671 (1994).

[15] D. E. McCumber and M. D. Sturge, Linewidth and temperature shift of the *R* lines in ruby, J. Appl. Phys. **34**, 1682 (1963).

[16] M. A. Krivoglaz, Theory of the phononless line broadening in the Mössbauer or optical spectrum, Sov. Phys. Solid State **6**, 1340 (1964).

[17] G. J. Small, Comment on frequency shift and transverse relaxation of optical transitions in organic solids, Chem. Phys. Lett. **57**, 501 (1978).

[18] I. S. Osad'ko, Optical dephasing and homogeneous optical bands in crystals and amorphous solids: Dynamic and stochastic approaches, Phys. Rep. **206**, 43 (1991).

[19] D. Hsu and J. L. Skinner, On the thermal broadening of zero-phonon impurity lines in absorption and fluorescence spectra, J. Chem. Phys. **81**, 1604 (1984).

[20] C. Clear, R. C. Schofield, K. D. Major, J. Iles-Smith, A. S. Clark, and D. P. S. McCutcheon, Phonon-induced optical dephasing in single organic molecules, Phys. Rev. Lett. **124**, 153602 (2020).

[21] M. Reitz, C. Sommer, B. Gurlek, V. Sandoghdar, D. Martin-Cano, and C. Genes, Molecule-photon interactions in phononic environments, Phys. Rev. Res. **2**, 033270 (2020).

[22] V. Hizhnyakov, Nonperturbative theory of zero-phonon transitions, Chem. Phys. Lett. **808**, 140092 (2022).

[23] T. Plakhotnik, M. W. Doherty, and N. B. Manson, Electron-phonon processes of the nitrogen-vacancy center in diamond, Phys. Rev. B **92**, 081203(R) (2015).

[24] M. Berg, C. A. Walsh, L. R. Narasimhan, K. A. Littau, and M. D. Fayer, Dynamics in low temperature glasses: Theory and experiments on optical dephasing, spectral diffusion, and hydrogen tunneling, J. Chem. Phys. **88**, 1564 (1988).

[25] Y. G. Vainer, M. A. Kol'chenko, A. V. Naumov, R. I. Personov, and S. J. Zilker, Photon echoes in doped organic amorphous systems over a wide (0.35–50 K) temperature range, J. Lumin. **86**, 265 (2000).

[26] G. Schulte, W. Grond, D. Haarer, and R. Silbey, Photochemical hole burning of phthalocyanine in polymer glasses: Thermal cycling and spectral diffusion, J. Chem. Phys. **88**, 679 (1988).

[27] Y. G. Vainer, A. V. Naumov, M. Bauer, and L. Kador, Experimental evidence of the local character of vibrations constituting the boson peak in amorphous solids, Phys. Rev. Lett. **97**, 185501 (2006).

[28] S. Völker, Hole-burning spectroscopy, Annu. Rev. Phys. Chem. **40**, 499 (1989).

[29] R. Jankowiak, H. Bässler, and R. Silbey, Verification of the importance of librational modes for optical dephasing in organic glasses, Chem. Phys. Lett. **125**, 139 (1986).
[30] B. Di Bartolo, *Optical Interactions in Solids* (World Scientific, Singapore, 2010).
[31] I. S. Osad'ko, *Selective Spectroscopy of Single Molecules* (Springer, Berlin, 2003).
[32] D. Hsu and J. L. Skinner, Nonperturbative theory of temperature-dependent optical dephasing in crystals. I. Acoustic or optical phonons, J. Chem. Phys. **81**, 5471 (1984).
[33] D. Hsu and J. L. Skinner, Nonperturbative theory of temperature-dependent optical dephasing in crystals. II. Pseudolocal phonons, J. Chem. Phys. **83**, 2097 (1985).
[34] T. Plakhotnik, E. A. Donley, and U. P. Wild, Single-molecule spectroscopy, Annu. Rev. Phys. Chem. **48**, 181 (1997).
[35] A. Naumov, I. Yu. Eremchev, and A. A. Gorshelev, Laser selective spectromicroscopy of myriad single molecules: Tool for far-field multicolour materials nanodiagnostics, Eur. Phys. J. D **68**, 348 (2014).
[36] I. Yu. Eremchev, A. V. Naumov, Yu. G. Vainer, and L. Kador, Effect of impurity molecules on the low-temperature vibrational dynamics of polyisobutylene: Investigation by single-molecule spectroscopy, J. Chem. Phys. **130**, 184507 (2009).
[37] N. Verdal and A. M. Kelley, Temperature dependence of phonon sidebands in line-narrowed fluorescence spectra of chromophores in glasses, J. Chem. Phys. **118**, 7985 (2003).
[38] L. R. Narasimhan, Y. S. Bai, M. A. Dugan, and M. D. Fayer, Observation of fast time scale spectral diffusion in a low temperature glass: Comparison of picosecond photon and stimulated echoes, Chem. Phys. Lett. **176**, 335 (1991).
[39] W. A. Phillips, Tunneling states in amorphous solids, J. Low Temp. Phys. **7**, 351 (1972).
[40] P. w. Anderson, B. I. Halperin, and C. M. Varma, Anomalous low-temperature thermal properties of glasses and spin glasses, Philos. Mag. **25**, 1 (1972).
[41] Y. G. Vainer, A. V. Naumov, M. A. Kol'chenko, and R. I. Personov, Quasi-localized low-frequency vibrational modes of disordered solids. I. Study by photon echo, Phys. Status Solidi B **241**, 3480 (2004).
[42] D. Hsu and J. L. Skinner, General quantum mechanical theory of pure dephasing, J. Lumin. **37**, 331 (1987).
[43] I. S. Osad'ko and S. A. Zhdanov, Effect of low-frequency modes on temperature broadening of optical lines of impurity centres in glasses, Opt. Commun. **42**, 185 (1982).
[44] O. N. Korotaev and M. Yu. Kaliteevskiĭ, Adiabatic mechanism of broadening of zero-phonon lines in impurity-crystal spectra, Sov. Phys. JETP **52**, 220 (1980).
[45] L. W. Molenkamp and D. A. Wiersma, Optical dephasing by uncorrelated phonon scattering to librations. An optical and picosecond photon echo study of a photosite of pentacene in benzoic acid, J. Chem. Phys. **80**, 3054 (1984).
[46] A. S. Barker and A. J. Sievers, Optical studies of the vibrational properties of disordered solids, Rev. Mod. Phys. **47**, S1 (1975).
[47] P. G. Dawber and R. J. Elliott, The vibrations of an atom of different mass in a cubic crystal, Proc. R. Soc. Lond. A. **273**, 222 (1963).
[48] P. D. Mannheim, Influence of force-constant changes on the lattice dynamics of cubic crystals with point defects, Phys. Rev. **165**, 1011 (1968).
[49] D. Hsu and J. L. Skinner, Nonperturbative theory of temperature-dependent optical dephasing in crystals. IV. Microscopic model for pseudolocal phonons, J. Chem. Phys. **87**, 54 (1987).
[50] W. Schirmacher, G. Diezemann, and C. Ganter, Harmonic vibrational excitations in disordered solids and the "boson" peak, Phys. Rev. Lett. **81**, 136 (1998).
[51] N. V. Surovtsev, S. V. Adichtchev, E. Rössler, and M. A. Ramos, Density of vibrational states and light-scattering coupling coefficient in the structural glass and glassy crystal of ethanol, J. Phys.: Condens. Matter **16**, 223 (2004).
[52] M. Rothenfusser, W. Dietsche, and H. Kinder, Linear dispersion of transverse high-frequency phonons in vitreous silica, Phys. Rev. B **27**, 5196 (1983).
[53] D. L. Huber, Reassessment of the Raman mechanism for homogeneous linewidths in glasses, J. Non-Cryst. Solids **51**, 241 (1982).
[54] I. Yu. Eremchev, M. Yu. Eremchev, and A. V. Naumov, Multifunctional far-field luminescence nanoscope for studying single molecules and quantum dots, Usp. Fiz. Nauk **189**, 312 (2019).
[55] I. Yu. Eremchev, A. Yu. Neliubov, K. N. Boldyrev, V. G. Ralchenko, V. S. Sedov, L. Kador, and A. V. Naumov, Microscopic insight into the inhomogeneous broadening of zero-phonon lines of GeV^- color centers in chemical vapor deposition diamond films synthesized from gaseous germane, J. Phys. Chem. C **125**, 17774 (2021).
[56] A.-M. Boiron, Ph. Tamarat, B. Lounis, R. Brown, and M. Orrit, Are the spectral trails of single molecules consistent with the standard two-level system model of glasses at low temperatures? Chem. Phys. **247**, 119 (1999).
[57] Y. I. Sobolev, A. V. Naumov, Y. G. Vainer, and L. Kador, Low temperature spectral dynamics of single molecules in ultrathin polymer films, J. Chem. Phys. **140**, 204907 (2014).
[58] E. Geva and J. L. Skinner, Theory of single-molecule optical line-shape distributions in low-temperature glasses, J. Phys. Chem. B **101**, 8920 (1997).
[59] A. V. Naumov, Y. G. Vainer, and L. Kador, Frequency dependence of the quadratic electron-phonon coupling constant in a polymer glass: Direct measurement by single-molecule spectroscopy, Phys. Rev. B **79**, 132201 (2009).
[60] A. Elschner, L. R. Narasimhan, and M. D. Fayer, High temperature optical dephasing mechanism for dye molecules in PMMA glass, Chem. Phys. Lett. **171**, 19 (1990).
[61] H. van der Laan, H. E. Smorenburg, Th. Schmidt, and S. Völker, Permanent hole burning with a diode laser: Excited-state dynamics of bacteriochlorophyll in glasses and micelles, J. Opt. Soc. Am. B **9**, 931 (1992).
[62] B. Frick, D. Richter, and S. Trevino, Inelastic fast relaxation in a weakly fragile polymer glass near Tg, Physica A **201**, 88 (1993).
[63] S. F. Parker, Inelastic neutron scattering spectra of polyethylene, J. Chem. Soc., Faraday Trans. **92**, 1941 (1996).
[64] J. Tomkinson, S. F. Parker, D. A. Braden, and B. S. Hudson, Inelastic neutron scattering spectra of the transverse acoustic modes of the normal alkanes, Phys. Chem. Chem. Phys. **4**, 716 (2002).
[65] A. Moradi, Z. Ristanović, M. Orrit, I. Deperasińska, and B. Kozankiewicz, Matrix-induced linear Stark effect of single

dibenzoterrylene molecules in 2,3-dibromonaphthalene crystal, ChemPhysChem **20**, 55 (2019).

[66] M. Orrit, J. Bernard, A. Zumbusch, and R. I. Personov, Stark effect on single molecules in a polymer matrix, Chem. Phys. Lett. **196**, 595 (1992).

[67] M. Białkowska, W. Chaładaj, I. Deperasińska, A. Drzewiecka-Antonik, A. E. Koziol, A. Makarewicz, and B. Kozankiewicz, Single molecules of terrylene in di-substituted naphthalenes crystallizing in the herringbone pattern, RSC Adv. **7**, 2780 (2017).

[68] M. González-Jiménez *et al.*, Understanding the emergence of the boson peak in molecular glasses, Nat. Commun. **14**, 215 (2023).

[69] G. Monaco and V. M. Giordano, Breakdown of the Debye approximation for the acoustic modes with nanometric wavelengths in glasses, Proc. Natl. Acad. Sci. **106**, 3659 (2009).

[70] P. Sheng, M. Zhou, and Z.-Q. Zhang, Phonon transport in strong-scattering media, Phys. Rev. Lett. **72**, 234 (1994).

[71] R. Kunz, K. Timpmann, J. Southall, R. J. Cogdell, A. Freiberg, and J. Köhler, Fluctuations in the electron–phonon coupling of a single chromoprotein, Angew. Chem. Int. Ed. **52**, 8726 (2013).

[72] E. A. Podshivaylov, M. A. Kniazeva, A. A. Gorshelev, I. Yu. Eremchev, A. V. Naumov, and P. A. Frantsuzov, Contribution of electron-phonon coupling to the luminescence spectra of single colloidal quantum dots, J. Chem. Phys. **151**, 174710 (2019).

[73] M. Klotz *et al.*, Prolonged orbital relaxation by locally modified phonon density of states for the Si V^- center in nanodiamonds, Phys. Rev. Lett. **128**, 153602 (2022).

[74] S. G. Bishop, J. P. Hadden, F. D. Alzahrani, R. Hekmati, D. L. Huffaker, W. W. Langbein, and A. J. Bennett, Room-temperature quantum emitter in aluminum nitride, ACS Photonics **7**, 1636 (2020).

[75] L. Razinkovas, M. W. Doherty, N. B. Manson, C. G. Van de Walle, and A. Alkauskas, Vibrational and vibronic structure of isolated point defects: The nitrogen-vacancy center in diamond, Phys. Rev. B **104**, 045303 (2021).

[76] K. Sharman, O. Golami, S. C. Wein, H. Zadeh-Haghighi, C. G. Rocha, A. Kubanek, and C. Simon, A DFT study of electron–phonon interactions for the C_2C_N and V_NN_B defects in hexagonal boron nitride: Investigating the role of the transition dipole direction, J. Phys.: Condens. Matter. **35**, 385701 (2023).

[77] T. Böttger, C. W. Thiel, Y. Sun, and R. L. Cone, Optical decoherence and spectral diffusion at 1.5 μm in Er^{3+}:Y_2SiO_5 versus magnetic field, temperature, and Er^{3+} concentration, Phys. Rev. B **73**, 075101 (2006).

[78] J. Tittel, R. Kettner, Th. Basché, C. Bräuchle, H. Quante, and K. Müllen, Spectral diffusion in an amorphous polymer probed by single molecule spectroscopy, J. Lumin. **64**, 1 (1995).

[79] A. V. Naumov, A. A. Gorshelev, Y. G. Vainer, L. Kador, and J. Köhler, Impurity spectroscopy at its ultimate limit: Relation between bulk spectrum, inhomogeneous broadening, and local disorder by spectroscopy of (nearly) all individual dopant molecules in solids, Phys. Chem. Chem. Phys. **13**, 1734 (2011).

[80] W. E. Moerner, T. Plakhotnik, T. Irngartinger, M. Croci, V. Palm, and U. P. Wild, Optical probing of single molecules of terrylene in a Shpol'kii matrix: A two-state single-molecule switch, J. Phys. Chem. **98**, 7382 (1994).